ChemPubSoc Europe

DOI: 10.1002/cbic.201300230

A Computational Study of the Effects of ^{13}C–^{13}C Scalar Couplings on ^{13}C CEST NMR Spectra: Towards Studies on a Uniformly ^{13}C-Labeled Protein

Pramodh Vallurupalli,[a] Guillaume Bouvignies,[a] and Lewis E. Kay*[a, b]

Dedicated to the memory of Professor Ivano Bertini and his infectious enthusiasm for life and science

Fifty years ago Forsen and Hoffman described an elegant experiment for quantifying the kinetics of chemical exchange between pairs of interconverting conformers.[1] In their simple approach a continuous wave (CW) radio frequency (rf) pulse was applied to longitudinal magnetization derived from one of the exchanging sites and the effect of the perturbation on magnetization from the second site was measured. Although initial applications focused on small organic molecules, subsequent studies were extended to protein systems as the sensitivity and resolution of NMR instrumentation improved.[2–5] These pioneering experiments showed that kinetics studies could be performed on complex molecules and further that the utility of the methodology could be extended to other applications such as the assignment of chemical shifts of one of the interconverting states, once the shifts in the second conformer were available.[2,6]

The basic principles of these early NMR experiments have been exploited to great advantage in MRI applications through so-called chemical exchange saturation transfer (CEST).[7,8] Here it has been recognized that the weak signals of metabolites that exchange protons with water can be amplified many fold by transferring magnetization from the metabolite to water and subsequently recording the water signal. Recently the MRI CEST experiment has been adapted to study chemical exchange between highly populated, long-lived ground ("visible") and sparsely populated, transiently formed ("invisible") excited states when they are in moderately slow exchange.[9–14]

In order to understand the basic features of this experiment that will be critical in what follows, we consider a spin exchanging between ground (G) and excited (E) states,

$$G \underset{k_{EG}}{\overset{k_{GE}}{\rightleftharpoons}} E$$

where the fractional population of E, p_E, is such that only resonances from the ground state are observed in NMR spectra.[10,15,16] The basic building block of the CEST experiment takes longitudinal magnetization and applies a weak CW rf field ($B_1 \sim 5$–50 Hz) for a duration T_{CEST} that is typically several hundreds of milliseconds. A series of experiments are recorded with the B_1 field applied at offsets that span the expected range for the spin probe in question (e.g., ^{15}N or ^{13}C). The intensity of the ground state cross peak, I, is measured for each B_1 offset by transferring the resultant z-magnetization into the transverse plane for detection. When the B_1 field is proximal to the ground state resonance, I decreases, as expected since the z-magnetization of state G is attenuated. In a similar manner, I decreases when the B_1 field is applied at the frequency of state E because the perturbation is transferred to the corresponding spin in the ground conformer through chemical exchange. The resulting CEST profiles, plotting I versus B_1 offset, therefore have intensity dips at ϖ_G and ϖ_E, corresponding to the resonance positions (in ppm) of ground and excited states; they can be analyzed to obtain exchange parameters, including $k_{ex} = k_{EG} + k_{GE}$, p_E and ϖ_E, as described previously.[10]

Protein applications of this methodology have focused on backbone ^{15}N, ^{1}HN $^{13}C\alpha$, ^{13}CO and side-chain methyl ^{13}C spins.[10–14] In the case of $^{13}C\alpha$ or methyl-carbon-based experiments,[12,14] proteins were labeled with isolated ^{13}C spins, avoiding homonuclear ^{13}C–^{13}C couplings which increase line widths of the dips in the CEST profiles, and consequently decrease resolution. In contrast, ^{13}CO experiments were recorded on a uniformly ^{13}C-labeled sample.[13] Attempts to decouple the $^{13}C\alpha$ spins from the ^{13}CO carbons in the CEST dimension were not successful because decoupling side-band artifacts were introduced, as described elsewhere,[13] and ultimately fully coupled data sets were obtained. The resultant one-bond ^{13}CO–$^{13}C\alpha$ couplings (51 Hz) could not be resolved in the CEST dimension with the B_1 fields that were used (≥ 20 Hz) and their effects were included in fits of the resulting CEST profiles, yielding accurate exchange parameters and chemical shifts.

Encouraged by our results using uniformly ^{13}C-labeled samples for ^{13}CO CEST experiments, we explore here the possibility of extending studies to aliphatic side-chain positions. Unlike the case for $^{13}C\alpha$ and ^{13}CO spins that are separated by over 100 ppm and hence are never strongly coupled, adjacent aliphatic side-chain carbons can have similar chemical shifts, leading to strong coupling conditions. Here we use simulations to investigate the feasibility of extracting accurate excited state ^{13}C chemical shifts in cases where probe nuclei are part of coupled ^{13}C–^{13}C spin networks, such as would be the case in uniformly ^{13}C-labeled protein samples. We show that for the B_1 fields that are used in experiments, ^{13}C–^{13}C couplings do not introduce errors in extracted chemical shifts, although in some cases the resulting CEST profiles can be affected. Excellent

[a] Dr. P. Vallurupalli, Dr. G. Bouvignies, Prof. L. E. Kay
Departments of Molecular Genetics, Biochemistry and Chemistry
University of Toronto
1, King's College Circle, Toronto, Ontario, M5S 1A8 (Canada)
E-mail: kay@pound.med.utoronto.ca

[b] Prof. L. E. Kay
Program in Molecular Structure and Function, Hospital for Sick Children
555 University Avenue, Toronto, Ontario, M5G 1X8 (Canada)

agreement is obtained between simulation and experiment, substantiating the results based on computation. The present study establishes the feasibility of obtaining accurate excited state aliphatic ^{13}C chemical shifts from CEST experiments recorded on fully ^{13}C-labeled proteins, paving the way for detailed structural studies of sparsely populated conformers using side-chain ^{13}C probes.

For the purposes of the simulations we consider here the simplest of molecular fragments, consisting of a pair of one-bond coupled ^{13}C-^{13}C spins with the value of J_{C1C2} set to 36 Hz, Figure 1 A, corresponding to the magnitude of aliphatic carbon couplings in proteins.[15,17] Further we suppose that the fragment is attached to a molecule that exchanges between states G and E, producing the spectrum shown in Figure 1 B, where ϖ_j^A is the chemical shift (ppm) of spin j in state A ($j \in \{'C1','C2'\}$, $A \in \{'G','E'\}$). Although the resonances from the excited state are typically not observed in spectra, they are shown here for the purpose of clarity. A schematic of a typical NMR experiment used to record CEST profiles is shown in Figure 1 C, omitting technical details that are not relevant for understanding basic concepts. In an actual experiment, magnetization is transferred from ^1H to ^{13}C, ^{13}C chemical shift is frequency encoded during a t_1 evolution period and magnetization restored to the z axis prior to the application of a weak CEST rf field, as described above.[12] The resultant longitudinal magnetization from state G (recall that state E is "invisible") is subsequently quantified by first transferring magnetizationn back to ^1H for detection and then measuring the intensity of the correlation at (ϖ_{C1}^G, ϖ_{H1}^G) in a 2D ^{13}C–^1H data set. By repeating the experiment as a function of position of the weak rf field, a CEST profile such as the one in Figure 1 D is obtained (using values of $p_E = 3.5\,\%$, $k_{ex} = 75\ s^{-1}$, $T_{CEST} = 250$ ms) where I and I_o are intensities of the ground state peak obtained in experiments recorded with and without the CEST interval, respectively. Note that dips at ϖ_G and ϖ_E are observed, as expected in the simple case of an "isolated" spin in exchange between a pair of sites.

Because a simple 2-spin ^{13}C–^{13}C fragment is considered here, there is no need to invoke the transfers from ^1H to ^{13}C and back in the simulations that follow. The t_1, t_2 evolution periods sandwiching the CEST interval can be taken into account simply by considering longitudinal magnetization originating on one of the carbon spins (C1 in what follows) prior to the CEST period, calculating evolution during the CEST interval using the Bloch–McConnell equations[18] describing two-site exchange[9,10] and then quantifying the longitudinal magnetization on C1 at the end of the CEST interval. Further ^1H–^{13}C scalar couplings during the CEST period can be ignored; in practice the effects of such couplings are eliminated by the application of ^1H decoupling.[10,12] The profiles in Figure 1 D–H were all calculated in this manner, with $J_{C1C2} = 0$ for Figure 1 D.

Next we set $J_{C1C2} = 36$ Hz and varied the difference in chemical shifts between carbons C1 and C2 (Hz), $\Delta^G = (\omega_{C2}^G - \omega_{C1}^G)/2\pi$ by moving the resonance frequency of C2, as described in the legend to Figure 1. Again the CEST profile of carbon C1 was simulated. For large values of $\Delta^G/J_{C1C2} > 10$, CEST profiles (e.g., Figure 1 E) show little difference relative to the case where $J_{C1C2} = 0$ (Figure 1 D) since the spin system is essentially weakly coupled. In principle, a doublet should be observed for each peak, separated by J_{C1C2}, however in practice the finite B_1 field used to perturb magnetization during the CEST interval broadens the dips in spectra and for B_1 fields ≥ 20 Hz resolved multiplet structure is not observed. Thus, the major difference between the profiles in Figure 1 D and E is the increased broadening caused by

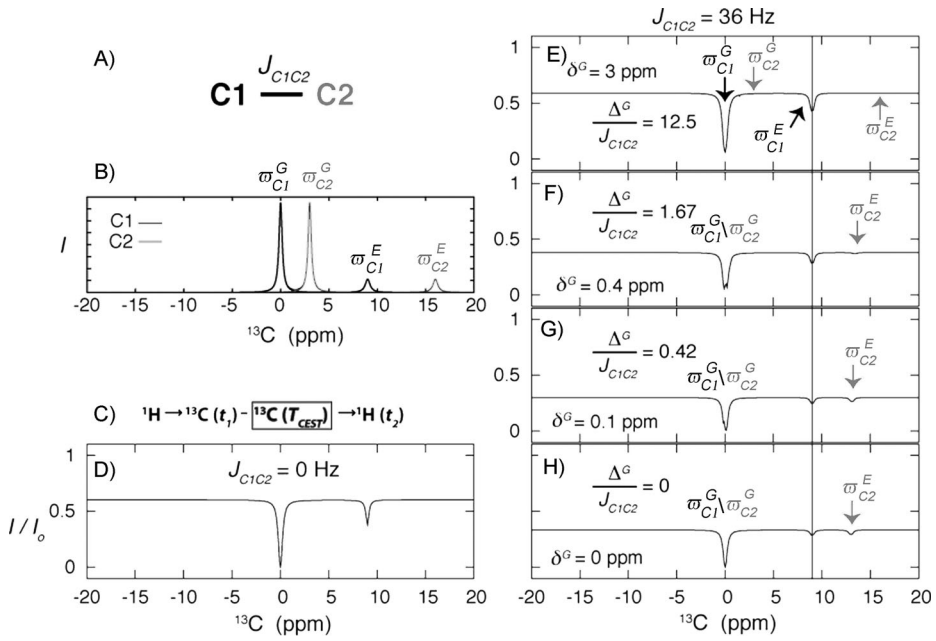

Figure 1. The effects of one bond ^{13}C–^{13}C scalar couplings on ^{13}C CEST profiles recorded on uniformly ^{13}C-labeled molecules. A) Two-spin ^{13}C–^{13}C spin-system comprising carbons C1 and C2 considered in simulations. J_{C1C2} is the one bond ^{13}C–^{13}C scalar-coupling constant. B) Spectrum of the spin system used: ϖ_{C1}^G and ϖ_{C2}^G are the chemical shifts (ppm) of C1 and C2 in the ground state, with the corresponding shifts in E given by ϖ_{C1}^E and ϖ_{C2}^E. Note that the excited state peaks are not normally visible in a conventional NMR spectrum and are shown here for clarity. The chemical shifts of C1 in G and E are 0 ppm and 9 ppm, respectively, while $\varpi_{C2}^G = \delta^G$ ppm and $\varpi_{C2}^E = \delta^G + 13$ ppm. The position of the ground state of C2 ($\delta^G = \varpi_{C2}^G - \varpi_{C1}^G$) is varied in panels E–H, keeping $\varpi_{C2}^E - \varpi_{C2}^G$ constant. C) Pulse scheme used to record CEST profiles, as described in the text. D–H) CEST profiles of carbon C1 obtained with $J_{C1C2} = 0$ Hz (D) or 36 Hz (E–H) and with the ratio Δ^G/J_{C1C2}, $\Delta^G = (\omega_{C2}^G - \omega_{C1}^G)/2\pi$, as indicated. A dip corresponding to the excited state chemical shift of C1 is always observed at the correct frequency, irrespective of Δ^G/J_{C1C2} (black vertical line). When δ^G is small (F–H) the CEST profile shows a dip at the excited state of carbon C2 (indicated by arrows). As described in the text, only C1 longitudinal magnetization is considered at the start and end of the 250 ms CEST interval. Values of $p_E = 3.5\,\%$, $k_{ex} = 75\ s^{-1}$ and $B_1 = 20$ Hz were used in all calculations.

the unresolved doublets for finite values of J_{C1C2} (Figure 1 E). As the Δ^G/J_{C1C2} ratio decreases (smaller values of Δ^G and $\delta^G = \varpi^G_{C2} - \varpi^G_{C1}$) the spin system becomes strongly coupled, yet the position of the excited state resonance of carbon C1 does not change (vertical line at ϖ^E_{C1}; Figure 1 F–H). This is a significant result because our main goal in using the ^{13}C CEST experiment is to measure accurate carbon chemical shifts of state *E* spins. As δ^G decreases, a dip at the resonance position of the ground state of C2 (ϖ^G_{C2}) starts to appear and for δ^G values of 0.4 (Figure 1 F) and 0.1 ppm (Figure 1 G), the proximity of the C1, C2 ground state resonances leads to an unresolved pair of lines close to 0 ppm. The appearance of ground state dips for both C1 and C2 is a "tell-tale" sign of strong coupling since in the weak coupling limit magnetization originating on C1 cannot flow to C2.[15] An additional dip also begins to appear at ϖ^E_{C2}, corresponding to the exchange of longitudinal magnetization between C1 of state G (denoted as C1(G)) and C2 of state E (C2(E)). This dip derives from a pathway whereby longitudinal magnetization C1(G) is transferred to C2(G) due to strong coupling, then to C2(E) through chemical exchange. The perturbation of longitudinal magnetization at C2(E) from the rf field, applied at the resonance position of the excited state of C2, is then transferred back to C1(G), decreasing its intensity. The increased length of the transfer pathway connecting C1(G) with C2(E) explains why the dip at ϖ^E_{C2} is smaller than at ϖ^E_{C1}, until $\Delta^G/J_{C1C2} = 0$ (Figure 1 H) when carbons 1 and 2 become indistinguishable so that the transfer between C1(G) and C2(G) is instantaneous. An additional point of interest is that the I/I_o ratio decreases from weak to strong coupling, reflecting the "leakage" of longitudinal magnetization from C1 to C2 during the CEST interval. Finally, it is worth noting that cases involving strong coupling will be known a priori from previously assigned ground state chemical shifts so that profiles of the sort indicated in Figure 1 involving additional dips can be predicted through simulations. In this manner, it is unlikely that the additional peaks observed would be interpreted incorrectly in the context of say a three-site exchange model which would also lead to additional dips relative to the case of interconversion involving a pair of sites.

Another interesting case is the "flip side" of what has been considered above, namely where C1 and C2 of the excited state are strongly coupled, while the corresponding carbons in the ground state are only weakly so, as illustrated in Figure 2. As with all the examples in Figure 1 the scheme of Figure 1 C is used so that the longitudinal magnetization of interest resides on the ground state of C1 both before and after the CEST interval. As expected, a dip is observed at the position of $\varpi^E_{C1}/\varpi^E_{C2}$ with an additional smaller dip at ϖ^G_{C2} that derives from a transfer scheme C1(G)→C1(E)→C2(E)→C2(G), where the middle transfer occurs through strong coupling and the other pair of transfers result from chemical exchange. The CEST rf field at ϖ^G_{C2} perturbs the magnetization of C2(G) and this perturbation is transferred back to C1(G), by reversing the pathway above, leading to a decrease in intensity of C1(G) that manifests in the small dip observed at the resonance position of the ground state of C2.

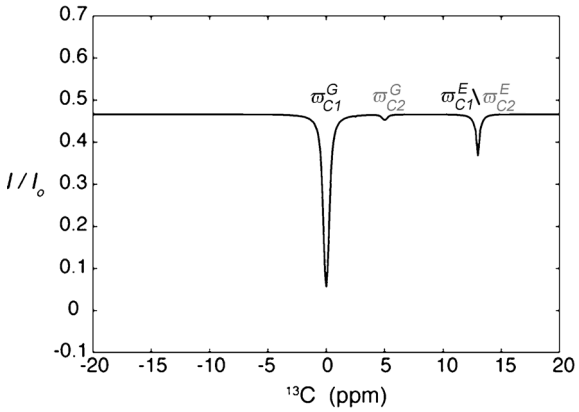

Figure 2. Strong coupling in the excited state can lead to extra dips in CEST profiles. Here we have set $\varpi^G_{C1} = 0$ ppm, $\varpi^G_{C2} = 5$ ppm, $\varpi^E_{C1} = \varpi^E_{C2} = 13$ ppm, so that C1 and C2 are strongly coupled in state E but not in G. An additional very small dip is noted at ϖ^G_{C2} in the CEST profile of carbon C1 that derives from a magnetization transfer pathway described in the text. All other parameters are as in Figure 1.

We have compared the results of simulations with those from experiment. Here we have used a uniformly ^{13}C-labeled sample of the G48A Fyn SH3 domain that interconverts between ground state folded and excited unfolded states, $k_{ex} = (120 \pm 15)\ s^{-1}$, $p_E = (5.8 \pm 0.2)\%$, 25 °C. The exchange parameters were measured using an ^{15}N-based CEST method,[10] which remains the preferred approach for obtaining rates and popu-

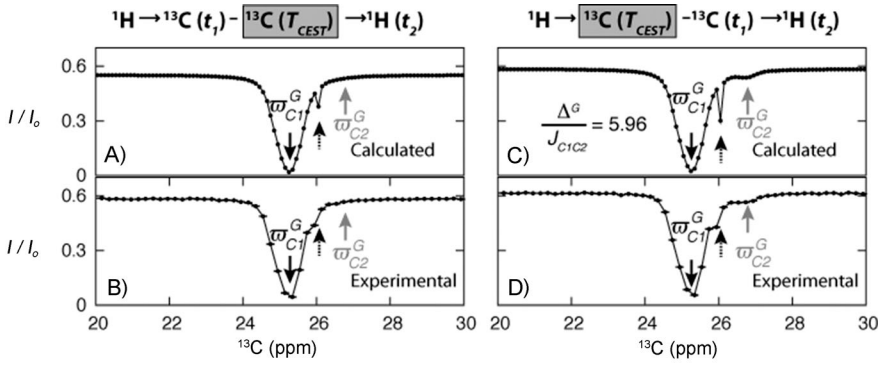

Figure 3. Validation of simulations through comparison with experiment. Calculated and experimental CEST profiles of Leu7 Cδ1 of the G48A Fyn SH3 domain using CEST experiments indicated schematically above the panels. The CEST profiles were calculated (A, C) using measured ground state chemical shifts $\varpi^G_{C\delta1} = 25.35$ ppm, $\varpi^G_{C\gamma} = 26.78$ ppm, and fitted excited state shifts $\varpi^E_{C\delta1} = 24.94$ ppm, $\varpi^E_{C\gamma} = 26.94$ ppm, $J_{C\delta1,C\gamma} = 36$ Hz, $k_{ex} = 120\ s^{-1}$, $p_E = 5.8\%$, $B_1 = 23.4$ Hz, $T_{CEST} = 250$ ms. All spectra show a major dip at ϖ^G_{C1} (black arrow) as well as a second smaller dip between the ground state chemical shifts of C1 (Cδ1) and C2 (Cγ) (dashed black arrow), as described in the text. In addition, the Scheme in which the CEST interval precedes t_1,t_2 (C, D) shows a further dip at ϖ^G_{C2} that is not present when the CEST period is flanked by the chemical shift evolution periods (A, B), see text. Relaxation rates used in the calculation are given in the Experimental Section and Computational Methods.

lations.[13] The calculated and experimentally measured ^{13}C CEST profiles for Leu7 Cδ1 (carbon C1) that is coupled to Cγ (carbon C2), with $\varpi^{G}_{C\delta1}=25.35$ ppm, $\varpi^{G}_{C\gamma}=26.78$ ppm, are shown in Figure 3. We have chosen this site because it is a representative example of the sorts of "artifacts" that can be seen in CEST spectra recorded on uniformly ^{13}C-labeled samples. Because Δ^{G}/J_{C1C2} is large (~6) we do not expect to see a dip corresponding to the excited state chemical shift of Cγ (ϖ^{E}_{C2}), based on the results of Figure 1, and indeed we do not. In fact, in no experimental cases for the Fyn SH3 domain were such dips observed. Figure 3A and B show the calculated (A) and experimental (B) profiles using the scheme where the CEST interval is between t_1 and t_2 evolution periods, as described previously. A small dip is predicted and observed at $0.5(\varpi^{G}_{C1}+\varpi^{G}_{C2})$ that reflects the transfer of magnetization between C1 and C2 due to a well-known Hartmann–Hahn effect.[19,20] Such a dip is also observed in Figure 1E but it is much smaller as the transfer efficiency decreases for larger Δ^{G} values. An isolated dip for the excited state C1 carbon is not observed, however, as $\varpi^{G}_{C1}\approx\varpi^{E}_{C1}$, that is the case for approximately 30% of the carbon spins in the Fyn SH3 domain. As an aside it is important to realize that in these cases the excited state carbon shifts can still of course be obtained, albeit likely at an accuracy that is lower than when resolved dips are measured. We have also simulated CEST profiles using a pulse scheme in which the CEST interval precedes both t_1 and t_2 evolution and compared the results with experiment (Figure 3C). Here longitudinal magnetization from both C1(G) and C2(G) must be considered initially since separation of C1 and C2 follows only after the CEST delay in this case. The small amount of transfer between C1(G) and C2(G) due to $\Delta^{G}/J_{C1C2}\sim6$ is sufficient to produce the small dip at ϖ^{G}_{C2} (Figure 3C and D), that derives from longitudinal magnetization initially on C2(G). This dip is not observed when the CEST period is flanked by t_1, t_2 because this version of the experiment specifically selects longitudinal magnetization from C1(G) at the beginning and end of the CEST element.[21] A dip at ϖ^{G}_{C2} would only be observed for a transfer such as C1(G)→C2(G)→C1(G) during the CEST interval, with each step the result of evolution due to strong coupling, and because Δ^{G}/J_{C1C2} is large, such a process is very inefficient. For applications involving uniformly ^{13}C-labeled proteins we prefer, therefore, to use the CEST experiment with the CEST element between the chemical shift evolution periods.

In summary, we have presented a computational study establishing that accurate values of excited state ^{13}C chemical shifts can be obtained from CEST experiments recorded on uniformly ^{13}C-labeled samples. For $\Delta^{G}/J_{C1C2}\geq2$, CEST profiles are essentially those expected in the limit that $J_{C1C2}=0$. For values smaller than ~1.5, additional dips can be observed but such cases are easily predicted using available chemical shifts, especially since aliphatic side-chain ^{13}C–^{13}C scalar couplings are well known (~35 Hz). Interestingly, for the G48A Fyn SH3 domain that we consider experimentally, $\Delta^{G}/J_{C1C2}>2.7$ for all residues, so it is clear that strong coupling effects are expected to be relatively rare in protein applications of the sort described here. Finally, results from computations have been verified experimentally using a pair of CEST pulse schemes. Importantly, experimental measurements on a uniformly ^{13}C-labeled sample of the G38A Fyn SH3 domain, to be published elsewhere, establish that accurate excited state shifts are obtained at all carbon sites, even for ^{13}C spins coupled to multiple partners (a scenario that is outside the scope of simulations considered here).The present study and related work[10,13] suggests that the great majority of heteroatom sites are accessible to study through CEST using a single ^{15}N,^{13}C-labeled sample, so long as the exchange time-scale is in the 20–300 s^{-1} range. In this regard CEST is unique compared to other NMR relaxation methods used to study excited protein states, including CPMG[22,23] or $R_{1\rho}$ relaxation dispersion[24] because a very weak B_1 field is used. The ability to measure excited state side-chain ^{13}C chemical shifts through CEST methodology addresses an important weakness in current relaxation dispersion experiments and promises to significantly extend studies of sparsely populated, transiently formed conformers.

Experimental Section and Computational Methods

All calculations were performed using an in-house developed program written in the Matlab v7.1 programming language (MathWorks Inc., Natick, MA). Evolution of magnetization during the CEST interval was calculated by solving the Liouville equation[25–27] [Eq. (1)]:

$$\frac{d}{dt}\rho=-i\hat{L}\rho \tag{1}$$

where ρ is the density matrix in Liouville space and $\hat{L}$ is the Liouvillian. The Liouvillian in turn was constructed from the Hamiltonian H [Eq. (2)][15]

$$H=\omega_{C1}C1_z+\omega_{C2}C2_z+2\pi J_{C1C2}(C1_xC2_x+C1_yC2_y+C1_zC2_z)+2\pi B_1(C1_x+C2_x) \tag{2}$$

where C1 and C2 denote carbons 1 and 2 respectively, as described in the text, $C1_j$ $j\in\{x,y,z\}$ is a spin angular momentum operator and ω_{Cj} is the offset (rad/sec) of the resonance position of carbon Cj from the frequency of application of the weak CW rf field (B_1 Hz) during the CEST period. It is convenient to first calculate H in the direct product (DP) basis set[15] ($|\alpha\alpha\rangle$, $|\alpha\beta\rangle$, $|\beta\alpha\rangle$, $|\beta\beta\rangle$). Next, the Liouvillian matrix (neglecting exchange for the moment, "NE") corresponding to H is calculated according to $\hat{L}^{H}_{DP,NE}=H\otimes E-E\otimes H'$ where E is a (4×4) identity matrix, H' is the transpose (i.e., $H_{ij}=H'_{ji}$) of the Hamiltonian matrix H and $\otimes$ is the tensor product operator.[27] In order to take into account the effects of spin relaxation most efficiently $\hat{L}^{H}_{DP,NE}$ was transformed into the product operator basis, generating $\hat{L}^{H}_{NE}$, with relaxation introduced by the relation, $\hat{L}_{NE}=\hat{L}^{H}_{NE}+\hat{L}^{R}_{NE}$ where $\hat{L}^{R}_{NE}$ consists of relaxation rates for the 16 different product operators that describe the evolution of the ^{13}C1–^{13}C2 spin system. These can in principle be calculated from Redfield theory[15,28] but here we have used empirical rates and have neglected cross-relaxation. Two-site chemical exchange is introduced through the standard Bloch–McConnell formalism[18,29] that results in a 31×31 Liouvillian matrix,[29,30] $\hat{L}$. We have assumed that only the chemical shift offsets of C1 and C2 differ between ground and excited states $\{(\omega^{G}_{C1},\omega^{G}_{C2}),(\omega^{E}_{C1},\omega^{E}_{C2})\}$ with all relaxation rates and $J_{C1,C2}$ identical. Equation (1) can be solved to obtain the

density matrix at the end of the CEST interval of duration T_{CEST}, $\rho(T_{CEST})$,

$$\rho(T_{CEST}) = e^{-i\hat{L}T_{CEST}}\rho(0) \quad (3)$$

where $\rho(0)$ is the density matrix at the start of the CEST period [Eq. (3)]. A set of calculations, each with a different rf carrier offset, is obtained, thereby generating the full CEST profile. B_1 inhomogeneity was included by performing each of the calculations for 11 different B_1 values, ranging from $B_1\times(1+2\sigma)$ to $B_1\times(1-2\sigma)$ where σ is the fractional B_1 field inhomogeneity, set to 0.1. The final CEST curve was obtained as a Gaussian (width σ) weighted sum of the 11 different calculations. Note that in all the calculations longitudinal and transverse relaxation rates of $R_1 = 1.9\ s^{-1}$, $R_2 = 8.4\ s^{-1}$, were used, a rate for multiple-quantum terms $R_{mq} = 15\ s^{-1}$ (such as, $2C1_xC2_y$) was employed and the relaxation of longitudinal order was set to $R_{zz} = 3.8\ s^{-1}$ ($2C1_zC2_z$). These rates are meant to approximate those relevant for the Fyn SH3 domain considered experimentally.

^{13}C CEST experiments (to be described elsewhere) were recorded on a 2 mM uniformly ^{15}N-, ^{13}C-labeled G48A Fyn SH3 domain sample dissolved in sodium phosphate buffer (50 mM, pH 7.0) containing EDTA (0.2 mM), 0.05% NaN_3 and H_2O/D_2O (9:1 *v/v*). Details of protein expression and purification were as described previously.[31,32] All data were recorded at 25 °C, 14.1 T. T_{CEST} was set to 250 ms during which a 23.4 Hz B_1 field was used.

Acknowledgements

The work was supported by grants from the Natural Sciences and Engineering Research Council of Canada and the Canadian Institutes of Health Research. L.E.K. holds a Canada Research Chair in Biochemistry.

Keywords: ^{13}C chemical shifts · chemical exchange saturation transfer · conformationally excited states · protein dynamics · scalar coupling effects

[1] S. Forsén, R. A. Hoffman, *J. Chem. Phys.* **1963**, *39*, 2892 – 2901.
[2] R. K. Gupta, A. G. Redfield, *Science* **1970**, *169*, 1204 – 1206.
[3] D. F. Hansen, J. J. Led, *Proc. Natl. Acad. Sci. USA* **2006**, *103*, 1738 – 1743.
[4] I. Bertini, S. Ciurli, A. Dikiy, R. Gasanov, C. Luchinat, G. Martini, N. Safarov, *J. Am. Chem. Soc.* **1999**, *121*, 2037 – 2046.
[5] P. J. Cayley, J. P. Albrand, J. Feeney, G. C. Roberts, E. A. Piper, A. S. Burgen, *Biochemistry* **1979**, *18*, 3886 – 3895.
[6] E. I. Hyde, B. Birdsall, G. C. K. Roberts, J. Feeney, A. S. V. Burgen, *Biochemistry* **1980**, *19*, 3738 – 3746.
[7] K. M. Ward, A. H. Aletras, R. S. Balaban, *J. Magn. Reson.* **2000**, *143*, 79 – 87.
[8] P. C. M. van Zijl, N. N. Yadav, *Magn. Reson. Med.* **2011**, *65*, 927 – 948.
[9] N. L. Fawzi, J. Ying, R. Ghirlando, D. A. Torchia, G. M. Clore, *Nature* **2011**, *480*, 268 – 272.
[10] P. Vallurupalli, G. Bouvignies, L. E. Kay, *J. Am. Chem. Soc.* **2012**, *134*, 8148 – 8161.
[11] G. Bouvignies, L. E. Kay, *J. Phys. Chem. B* **2012**, *116*, 14311 – 14317.
[12] G. Bouvignies, L. E. Kay, *J. Biomol. NMR* **2012**, *53*, 303 – 310.
[13] P. Vallurupalli, L. E. Kay, *Angew. Chem.* **2013**, *125*, 4250 – 4253; *Angew. Chem. Int. Ed.* **2013**, *52*, 4156 – 4159.
[14] A. L. Hansen, G. Bouvignies, L. E. Kay, *J. Biomol. NMR* **2013**, *55*, 279 – 289.
[15] J. Cavanagh, W. J. Fairbrother, A. G. Palmer, M. Rance, N. J. Skelton in *Protein NMR Spectroscopy, Principles and Practice*, 2nd ed., Academic Press, San Diego, **2006**.
[16] A. G. Palmer III, *Chem. Rev.* **2004**, *104*, 3623 – 3640.
[17] V. F. Bystrov, *Prog. Nucl. Magn. Reson. Spectrosc.* **1976**, *10*, 41 – 82.
[18] H. M. McConnell, *J. Chem. Phys.* **1958**, *28*, 430 – 431.
[19] S. R. Hartmann, E. L. Hahn, *Phys. Rev.* **1962**, *128*, 2042 – 2053.
[20] L. Müller, R. R. Ernst, *Mol. Phys.* **1979**, *38*, 963 – 992.
[21] R. Ishima, D. A. Torchia, *J. Biomol. NMR* **2003**, *25*, 243 – 248.
[22] D. F. Hansen, P. Vallurupalli, P. Lundstrom, P. Neudecker, L. E. Kay, *J. Am. Chem. Soc.* **2008**, *130*, 2667 – 2675.
[23] A. G. Palmer III, C. D. Kroenke, J. P. Loria, *Methods Enzymol.* **2001**, *339*, 204 – 238.
[24] A. G. Palmer, F. Massi, *Chem. Rev.* **2006**, *106*, 1700 – 1719.
[25] R. Ghose, *Concepts Magn. Reson.* **2000**, *12*, 152 – 172.
[26] A. D. Bain, B. Berno, *Prog. Nucl. Magn. Reson. Spectrosc.* **2011**, *59*, 223 – 244.
[27] R. R. Ernst, G. Bodenhausen, A. Wokaun in *Principles of Nuclear Magnetic Resonance in One and Two Dimensions*, 1st ed., Oxford Science Publications, Oxford, **1987**.
[28] A. G. Redfield, *IBM J. Res. Dev.* **1957**, *1*, 19 – 31.
[29] P. Allard, M. Helgstrand, T. Hard, *J. Magn. Reson.* **1998**, *134*, 7 – 16.
[30] M. H. Levitt, L. Dibari, *Phys. Rev. Lett.* **1992**, *69*, 3124 – 3127.
[31] A. M. Ruschak, T. L. Religa, S. Breuer, S. Witt, L. E. Kay, *Nature* **2010**, *467*, 868 – 871.
[32] A. A. Di Nardo, D. M. Korzhnev, P. J. Stogios, A. Zarrine-Afsar, L. E. Kay, A. R. Davidson, *Proc. Natl. Acad. Sci. USA* **2004**, *101*, 7954 – 7959.

Received: April 12, 2013
Published online on June 19, 2013